Progress Report on the Tohoku CYRIC Neutron TOF Facitities

I. 20 Progress Report on the Tohoku CYRIC Neutron TOF Facilities

Orihara H., Nishihara S.*, Furukawa K.**, Kabasawa M.***, Kawamura T.***,
Takahashi Y.***, Maeda K.**** and Nakagawa T.***
Cyclotron and Radioisotope Center, Tohoku University
Mitsubishi Electric Corporation*
National Laboratory of High Energy Physics**
Department of Physics, Faculty of Science, Tohoku University***
College of General Education, Tohoku University****

The first phase of the CYRIC neutron time-of-flight (TOF) facilities finished in 1980.[1] With a successful operation of the facilities, in which a large volume neutron detector located at a flight path of 24 m and NIM standard electronics modules capable for four dimentional (TOF, light-out put, position of light event and n-γ discrimination) data aquisition were equipped, a number of the low-energy (p,n) works have been carried out. In parallel with these activities, developments of facilities have been made. As pointed out in ref. 1, the progress in the data aquisition system was of particular importance, since it allowed us the efficient use of beam time even with a longer neutron flight path up to 44 m. Since the end of 1985, the use of twelve pieces of the large volume neutron detector has been available. In particular, the efficiency of the neutron counter has been calibrated absolutely by comparing the neutrons from the $^{7}Li(p,n)^{7}Be$ reaction with absolute neutron fluence determined by the activation technique. In this report, we describe the CAMAC based new data aquisition system and the neutron detection efficiency.

Neutron Detector

Two types of neutron detector are now used to pick-up the signals for neutron arrival. One is the same type as described in ref. 1, having dimentions shown in fig. 1 and being filled with liquid scintillator NE213 which has good performance for the n-γ discrimination. The other one is circular type with NE213 container of 8" in diameter and of 5 cm in depth, to which a 5"ϕ Hamamatsu photomultiplier is equipped. In the latter case, it is needless to measure the position for a light event in the detector, making the electronic diagram much simpler. It was found that there was no significant difference in the time resolution between these two types of the neutron detector.

Electronics and Data Aquisition System

Figure 2 and 3 show the diagrams of the electronics for the rectangular

and circular shaped neutron detectors, respectively. M.T. denotes the mean timer equalize the photon transit time, independent of where the light event occur, by providing an output pulse at always a fixed time, VDC means voltage to digital converter which digitize light out-put signal, and QDC is the charge to digital converter. The other notations in the figures should be self-explanatory. There used two methods for n-γ discrimination. In fig. 2 the pulse shape discriminator pick-up the rise-time of the anode pulse in PMT, and the TDC digitize the time difference of timing signals betwen PSD and CFD, while, in fig. 3, a pulse height from the slow-component of the anode pulse (partial light-output) is compared with that from total light output in order to obtain the information of n-γ discrimination. The CAMAC standard modules such as TDC shown in fig. 4 are mounted in the CAMAC crate located at the detector site, and they are locally controlled by an A2 type crate controller, which accepts external commands from the branch highway as well. The CAMAC Booster (CAB) accepts digital data through receiver transmitters. It plays a role of branch driver by containing a fast bit-slice micro-processor. In the present system, CAB selects a reasonable data and condense the data into half-size. The time needed for processing an event is about 140 micro-second including the conversion time in ADC. Figure 5 shows the diagram of CYRIC PDP11/44 data processing system. The digital data, thus obtained, is sent to the host computer through a crate controller at a rate of ∿200 kiro-bite per second. During a run, TOF, light and n-γ discrimination spectra for each detector are stored in a data area in the host computer, together with TOF spectra gated by the light and n-γ discrimination signals, and neutron energy spectrum versus excitation energies in the residual nucleus are ready for being monitored. Various kinds of spectrum up to 160 are available in the present data aquisition system for on-line monitoring.

Detector Efficiency Calibration

In the previous report[1] we have shown a preliminary result for the efficiency calibrated for the presently discussed rectangular shape neutron detector. In ref. 1 neutron yields at θ_L = 0° and 3.5° were normalized to the absolute cross sections reported by Poppe et al.[2] and Schery et al.[3] In the present report we describe a systematic study for the efficiency and the determination of absolute neutron fluence by activation technique. The efficiency depends both on the neutron energy and the threshold energy which is settled by software to avoide the overlap of neutron spectra in a TOF measurement with the limitted length of a beam pulse interval.

Figure 6 shows a neutron energy spectrum obtained from the $^{9}Be(p,n)^{9}B$ reaction at E_p = 35 MeV with a thick target. Response functions of the neutron detector for monochromatic neutrons, which have been selected from the above mentioned continuous energy neutrons by means of the TOF technique, are shown in fig. 7. Abscissa is in unit of electron energy. Each response curve has an edge corresponding to the maximum recoil energy in the n-p scattering.

A similar edge by compton scattering is seen when we measure the response function for a monochromatic γ-ray. It is convenient to find the relationship between neutron and γ-ray energies which give the same amount of light outputs from the NE213 liquid scintillator. We have obtained such a calibration curve, as was firstly presented by Verbinski et al.[4], which gives us an estimation that the maximum light output by an 8.5 MeV neutron is identical to that by γ-ray, compton scattered electron energy by which is ∿5 MeV (see fig. 7). This calibration curve is readily used for setting the neutron threshold energy by the measurement of γ-ray spectrum instead of the monochromatic neutron spectrum prior to an usual experiment of neutron analysis.

On the other hand, the integration of a response function at a fixed threshod energy gives us a measure of the efficiency for a monochromatic neutron. Furthermore, it is well known that a response function is well reproduced by the Monte-Carlo calculation. We have carried out Monte-Carlo simulation, by taking into accounts neutron scattering by proton and carbon, (n,n'), (n,p), (n,d) and (n,α) on ^{12}C, etc., an example for which is illustrated in fig. 8. The efficiency obtained by the Monte-Carlo calculation was checked by the measurement of absolute fluence of 34 MeV-neutron. Angular distributions of emitted neutrons from the $^{7}Li(p,n)^{7}Be$ reaction at E_p = 35 MeV leading to the ground and first excited states in ^{7}Be were measured as a part of this work as shown in fig. 9. Note that only the relative angular distribution is needed for the present purpose. Following the overnight (12 hr) proton irradiation, which was short enough time comparing to the half-life of ^{7}Be (53.3 d), to measure the angular distributions, the ammount of ^{7}Be produced was determined to be 1.27 μCi by observing 0.478 MeV γ-rays from a 10.4% branch of ^{7}Be. Thus we obtained absolute neutron fluence by which the detection efficiency is determined by comparing with number of neutrons counted. Note that no measurements of beam currents or target thickness are required. The comparison between the efficiencies at E_n = 34 MeV obtained from the Monte-Carlo calculation and the activation method is quite satisfactory. Figure 10 illustrates neutron detection efficiencies as a function of the neutron energy with a parameter of the threshold energy ranging 1.2 through 10.0 MeV by 0.4 MeV step. The absolute cross sections in fig. 9 were obtained by using these efficiencies. It is plausible to point out that the absolute differential cross sections in fig. 8 are quite consistent with those numerically reported in ref. 3 by Schery et al.

We have finished the construction and improvement of the new TOF facilities which allow us a high-resolution and high-efficiency measurement for neutron detection experiments. The forthcoming phase of these facilities may contain the developments capable for the neutron induced reactions.

This work was partly supported by Grant-in-Aid for Scientific Research, No. 57540132 and No. 59540147, from the Ministry of Education, Science and Culture in Japan.

References

1) Orihara H. and Murakami T., Nucl. Instrum. Methods 188 (1981) 15.
2) Shery S. D. et al., Nucl. Instrum. Methods 147 (1977) 399.
3) Poppe C. H. et al., Phys. Rev. C 14 (1976) 438.
4) Verbinski V. V. et al., Nucl. Instrum. Methods 65 (1968) 8.

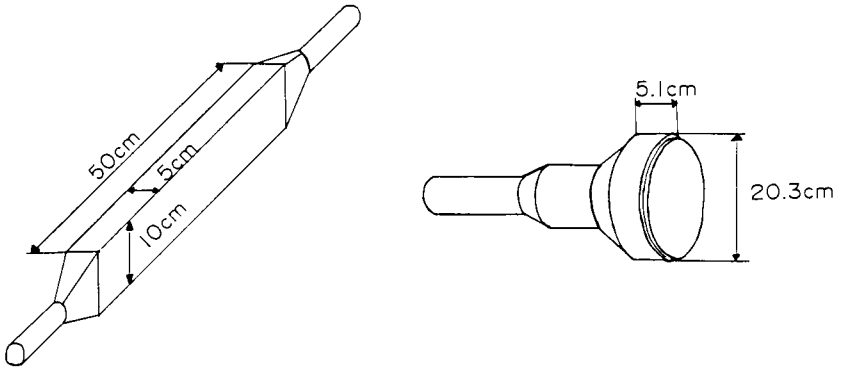

Fig. 1. Two kinds of presently tested neutron detector. One in left hand of the figure is lectangular shaped detector similarly designed as that discussed in ref. 1, while one in the bottom is the new detector with a 5" photomultiplier.

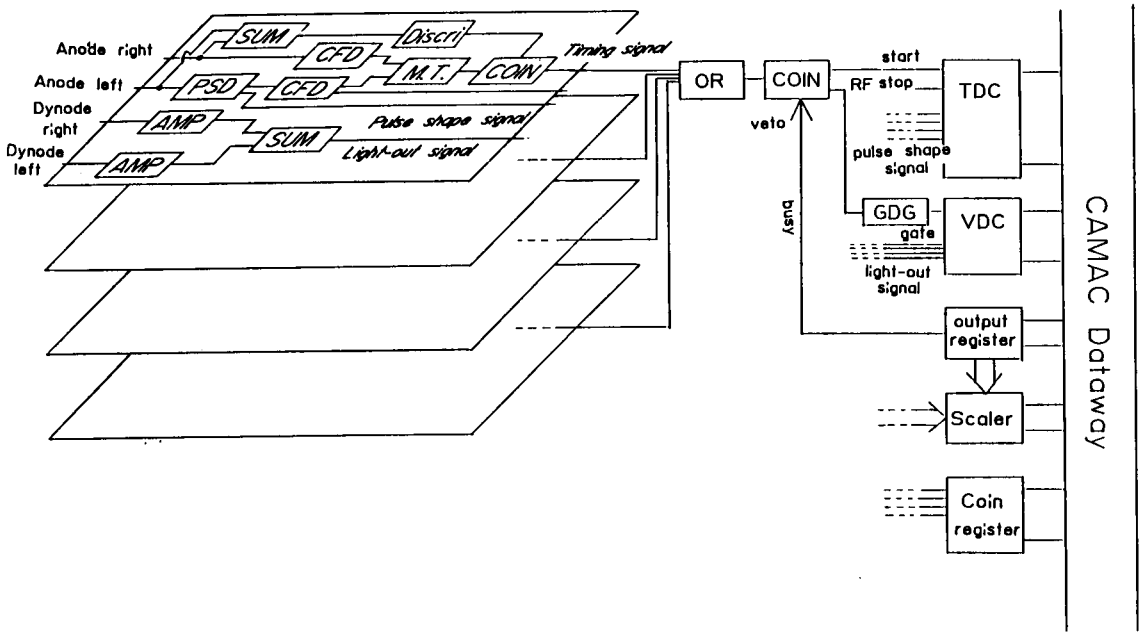

Fig. 2. Electronic set-up for TOF measurements with four rectangular shaped detectors.

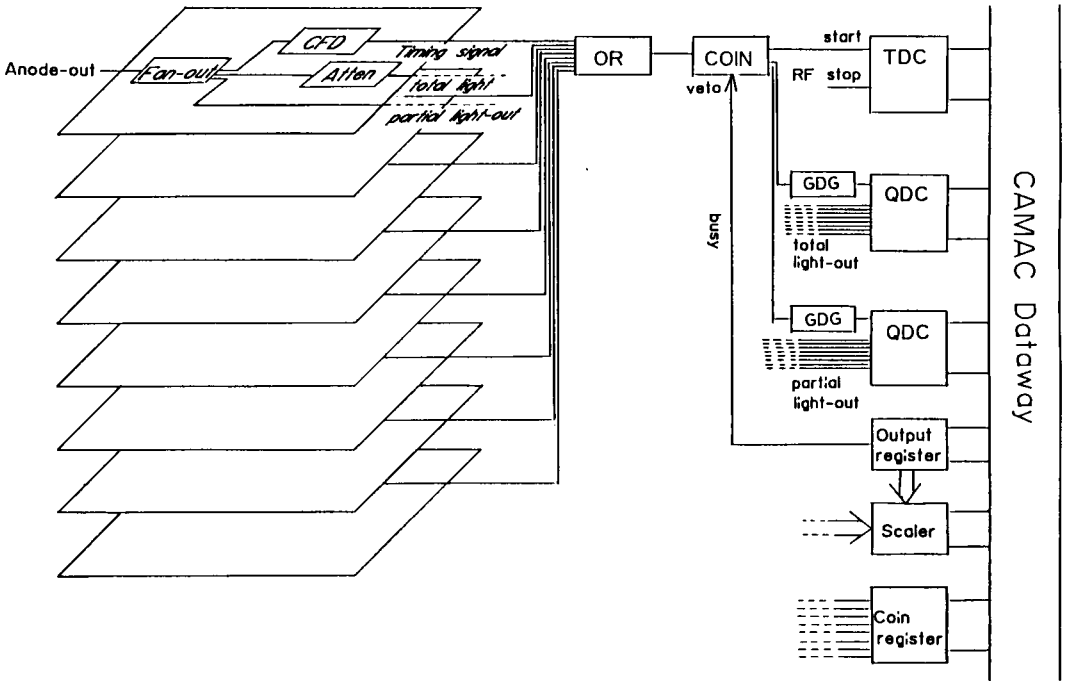

Fig. 3. Same with fig. 2, but for the eight circular shaped detectors.

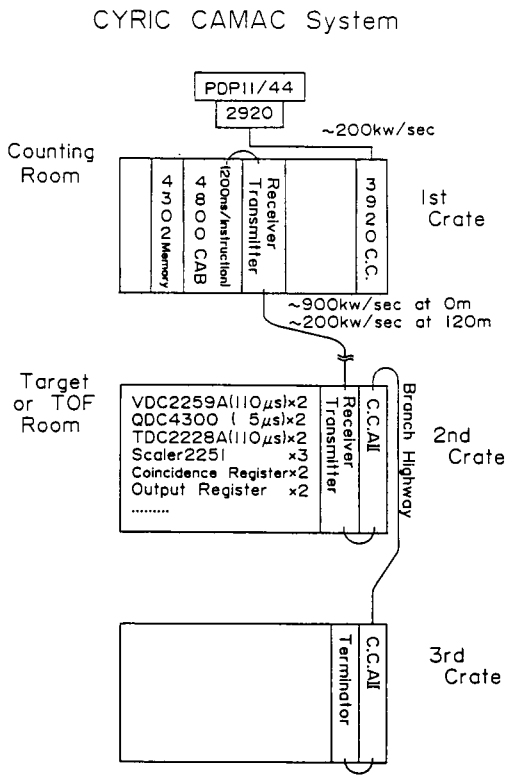

Fig. 4. CAMAC standard data acquisition system.

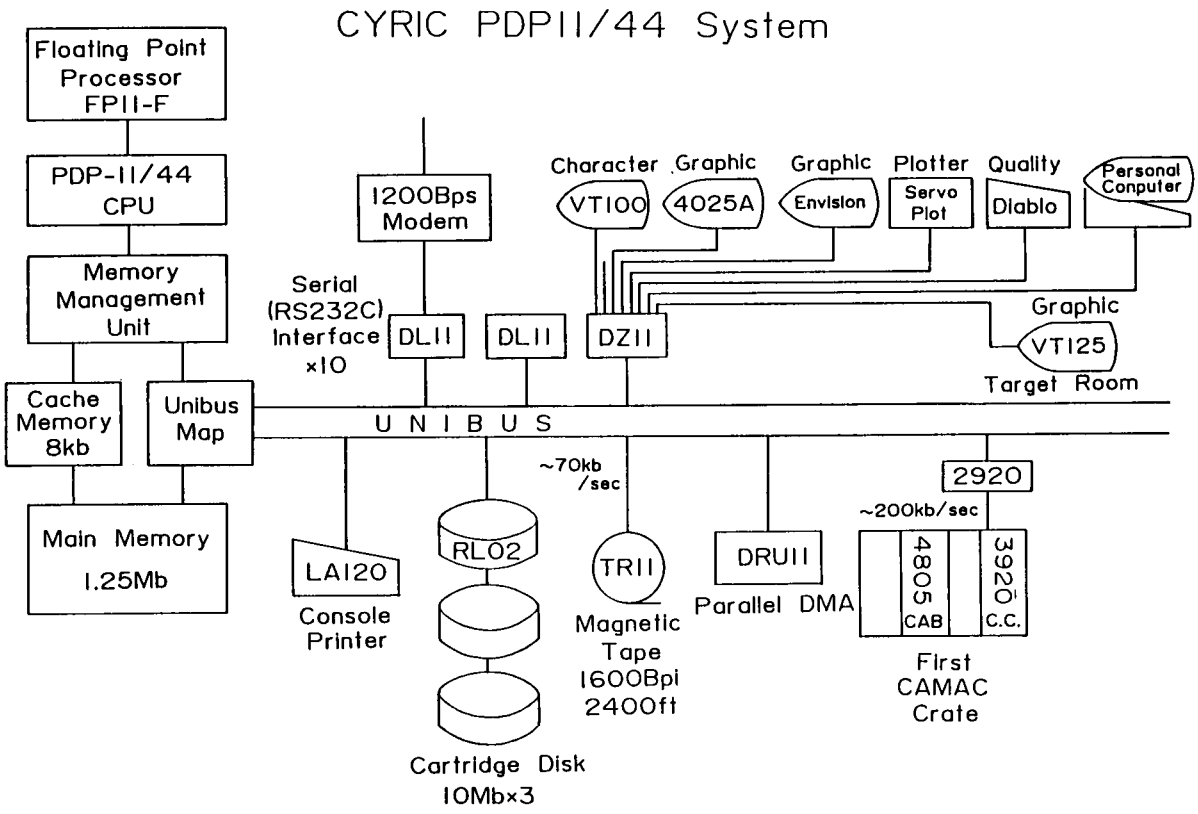

Fig. 5. CYRIC PDP11/44 data processing system.

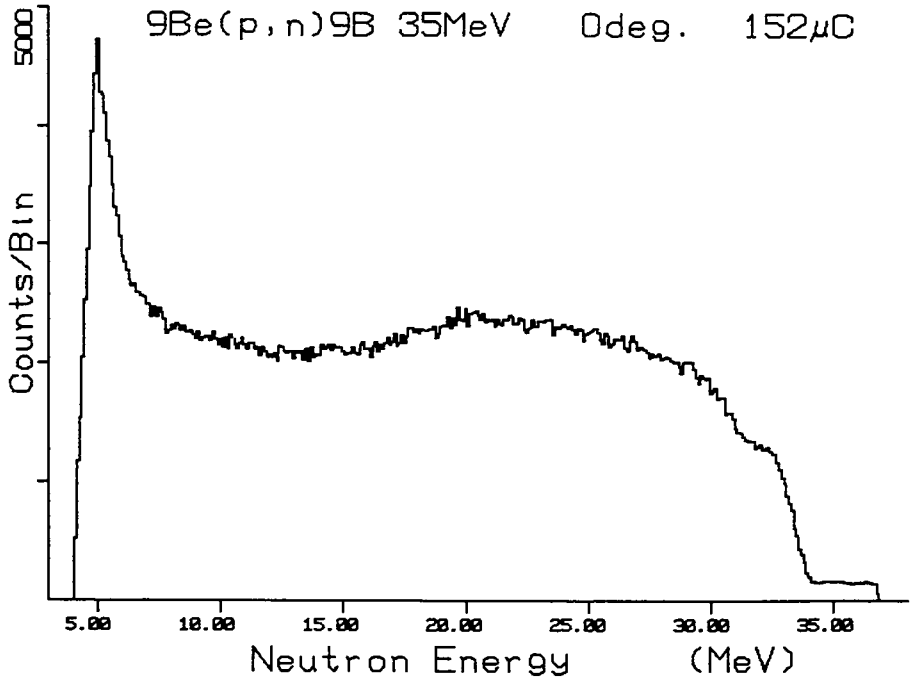

Fig. 6. Neutron energy spectrum from the $^{9}Be(p,n)^{9}B$ reaction at E_p = 35 MeV taken with thick Be target.

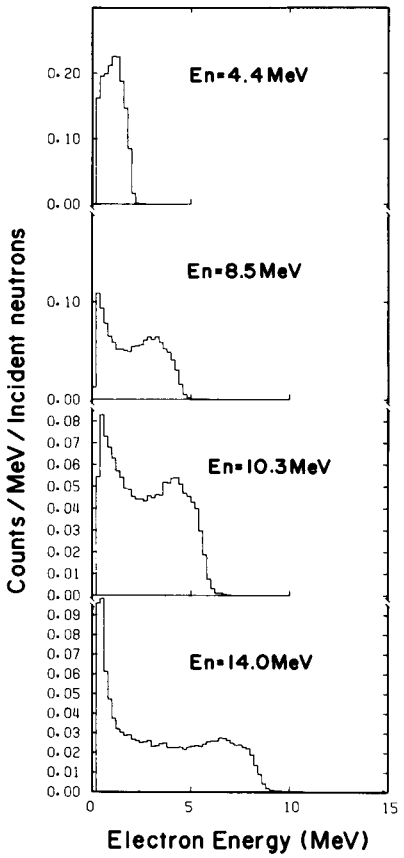

Fig. 7. Response function of the presently tested neutron detector (rectangular) for monochromatic neutrons selected by TOF technique from the continuum neutrons in fig. 6. The neutron threshold energy is settled as low as possible.

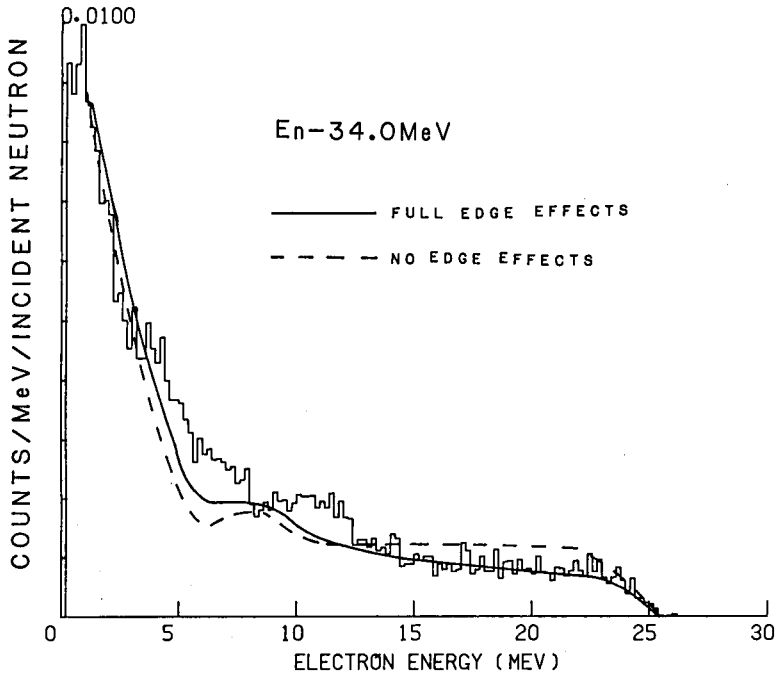

Fig. 8. The response function for 34-MeV neutrons. Curves in the figure are Monte-Carlo calculations.

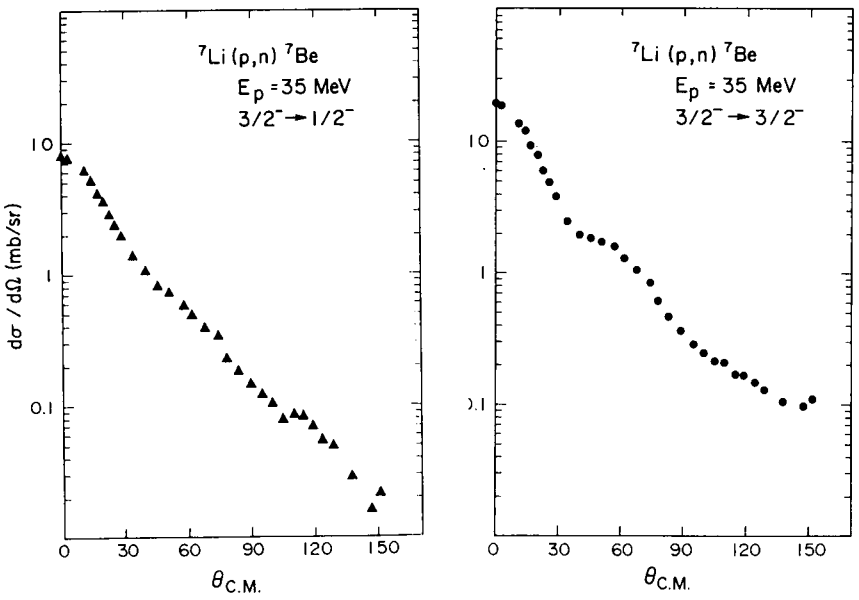

Fig. 9. Angular distribution of neutrons from the ^{7}Li(p,n)^{7}Be reaction leading to the ground and first excited states in ^{7}Be. Angular distributions were used for the efficiency determination by the activation technique, while the absolute cross sections were calibrated by the present study.

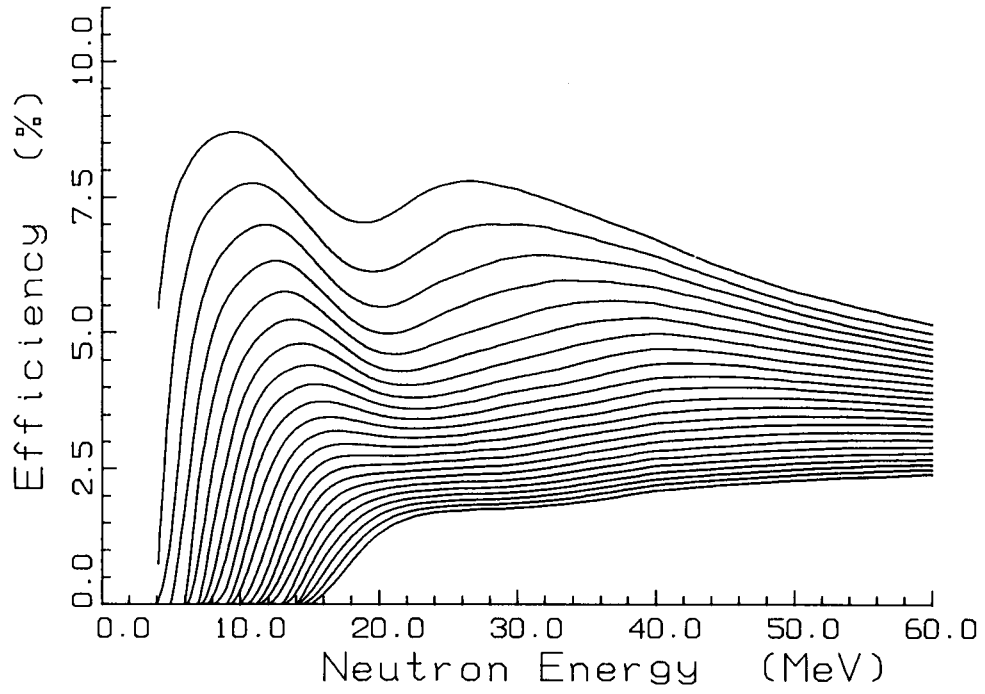

Fig. 10. Detection efficiencies for neutrons with a parameter of the neutron threshold energy.